Defect Detection Capabilities of Barker-Coded Thermal Wave Imaging in Titanium Alloy (Ti-6AL-4V)

Anshul Sharma[1], Vanita Arora[2], Ishant Singh[1], Priyanka Das[1] Ravibabu Mulaveesala[1a]

[1]InfraRed Imaging Laboratory (IRIL) Laboratory, Centre for Sensors, Instrumentation and cyber-physical Systems Engineering (SeNSE), Indian Institute of Technology Delhi, Hauz Khas, New Delhi-110016, India
[2]Indian Institute of Information Technology Una, Vill. Saloh, Teh. Haroli, Distt. Una Himachal Pradesh, India-177209.
[a]*Email: mulaveesala@sense.iitd.ac.in*

Abstract

Pulse compression favorable active infrared thermographic techniques have emerged as highly promising evaluation methodologies among various thermal non-destructive testing and imaging modalities for identifying subsurface anomalies in the test specimen. Because they outperform commonly utilized pulse and periodically modulation-based conventional thermal wave imaging modalities regarding defect detection sensitivity and resolution while employing low peak power heat sources and a comparatively moderate amount of experimenting time. Recently proposed Barker-Coded Thermal Wave Imaging (BCTWI) has offered these advantages over other infrared thermographic techniques. Several data processing methodologies are also be developing to characterize the anomalies from the depicted thermal data. This study highly recommends pulse compression-based data processing approaches for the Barker-coded thermal wave imaging technique. This is because it enhances the localization of supplied thermal energy into the main lobe of cross-correlation data and dispenses significantly less energy into the sidelobes. Current study focused on the application of BCTWI modality with time domain-based and frequency domain data processing approaches such as time domain correlation, time domain phase and frequency domain phase analysis for defect detection in Titanium alloy (Ti-6Al-4V). The results show that the pulse compression-based time domain analysis of the captured thermal data over the test specimen has improved the visibility, contrast, and detectability of the anomalies regarding the frequency domain. Further, the findings depicted using the various approaches have been contrasted using the correlation coefficient as the figures of merit.

Keywords: *Barker-Coded Thermal Wave Imaging (BCTWI); Pulse compression; Titanium alloy (Ti-6Al-4V); signal-to-noise ratio; correlation coefficient*

1 Introduction

Recent technological advancements have seen a huge surge in the usage of titanium-based alloys in different sectors such as in industrial applications, aerospace, medical implants, marine, and automotive construction. Titanium alloys offer certain unique properties including high strength-to-weight ratio, corrosion resistance, and biocompatibility [1, 2]. However, during the production and manufacturing of titanium alloys, there might exist the probability of an unavoidable delamination or occurrence of sub-surface defects. This leads to severe disruption in the architectural uniformity and in-service application of the product and can negatively impact the native properties and overall performance of the manufactured material. Out of the various titanium alloys, Ti-6Al-4V is one of the most commonly used alloys, which contains 6% of aluminium and 4% of vanadium in its composition and showcase lightweight, high stiffness, and high resistance properties for usage [1]. In case of Ti-6Al-4V titanium alloy, defects can arise at both the surface or

sub-surface level due to several reasons which include improper heat treatment, welding, machining, casting, or finishing of surface of the material [2]. Common defects generated during the Ti-6Al-4V titanium alloy production include porosity, inclusions, cracks, surface and subsurface defects, which define the irregularities or imperfections of the material surface which hampers the appearance, roughness, and performance of the product. Hence, detecting and evaluating any defect in real-time within the manufactured titanium-based alloy material is crucial to ensure the quality and reliability of the final product formed before its usage in various application domains [1-6].

For the purpose of defect detection via a non-destructive, non-contact, and real-time testing methodology without damaging or affecting the material properties, several common non-destructive testing (NDT) techniques are being employed widely for characterizing Ti-6Al-4V titanium alloy [1, 2]. These techniques include: X-ray radiography [1, 2], ultrasonic testing [3], eddy current testing [4], and magnetic particle testing [5]. In the last few decades, infrared thermographic testing [7-19] has emerged as a potent and reliable defect detection modality in various industrial and medical sectors. Infrared thermography is a rapidly emerging technique which evaluates a rapid and real-time defect detection by observing the thermal inhomogeneities within the testing material. The presence of thermal inhomogeneities causes in the disturbances in the surface bounded thermal propagation and impedes the diffusion of heat across the material to identify defects such as cracks, voids, inclusions, or delamination. This ultimately results in the temperature variation over the defective surface in comparison to that observed for the non-defective region of the material. This type of temperature contrast is observed directly by the infrared camera at precise locations of the material being monitored. Various conventional thermographic techniques are used for defect detection in titanium alloys, which include pulsed thermography (PT) [7-13], lock-in thermography (LT) [14-16], and Pulse phase thermography (PPT) [17-19]. Each technique has its advantages and limitations.

Pulse thermography provides better resolution and is a fast technique because short-duration high peak power is utilized in this technique to experiment. So, to acquire higher resolution and probe a high band of frequencies in the test specimen, high peak power heat sources are required, which is the main limitation of pulse-based thermographic techniques (PT and PPT). On the contrary, in lock-in thermography, there is no such requirement for high peak power sources, but due to the fixed frequency used in the sinusoidal excitation limits the depth resolution. This can be improved by repeating experimentation, which is time-consuming [7-19]. So, to overcome all the limitations associated with these conventional thermographic techniques (PT, LT, and PPT), the current work highlights the defect detection capability of barker-coded thermal wave imaging (BCTWI) modality [20-22]. This has been followed up by modeling a numerical model of Titanium alloy Ti-6Al-4V with 25 flat bottom holes under adiabatic boundary conditions with constant initial conditions. The 7-bit Barker coded thermal excitation is used to illuminate the sample surface, and a corresponding thermal pattern has been recorded. This recorded data is then processed with the frequency and time domain-based data processing approaches to analyse the proposed technique's subsurface defect detection capability. Further, the defect depth scanning capability of the proposed scheme is illustrated by considering the time domain correlation coefficient as a figure of merit.

2 Theory

2.1 Barker coded excitation

Compared to other modulation methodologies, the Barker-coded method is the most straightforward binary phase code, with the least compression side lobes. Moreover, this code's autocorrelation feature provides a proportionate compression ratio to the code's length. However, choosing the correct code length requires balancing the time needed for experimentation and the requirement for side lobe minimization. In thermography, lengthy testing reduces the technique's advantages, but shorter experiments may require high peak power heat sources. The best solution, thus, is achieved by using an appropriate code length and experimental period. This current study emphasizes the suggested technique's detection capabilities using a 7-bit code length that provides the lowest compression ratio of any other code length, as shown in figure.1 [20-22].

2.2 Coded excitation thermal waves solution for a finite system:

To study the thermal waves generated by the incident-coded excitation are analysed by a one-

dimensional Fourier heat equation given as follows [23-27]:

$$\frac{\partial^2 U(x,t)}{\partial x^2} - \frac{1}{\alpha}\frac{\partial U(x,t)}{\partial t} = 0 \qquad (1)$$

where, z_1,, z,, z_2; $\tau > 0$

where $U(x,\tau)$ temporal thermal distribution over the test specimen surface at location x at time t; Specimen thermal diffusivity has been represented by $\alpha = (k/\rho c)$; k -Thermal conductivity; ρ - Specimen Density; c - Specific heat of the specimen.

The temporal thermal distribution over the test specimen surface (at $x = 0$) is obtained by solving Eq. (1) under the 7-bit Barker coded excitation with a peak power Q_o (figure.1) with adiabatic boundary conditions and constant initial conditions. The current excitation used for this thermographic study is the measure of the combination of delayed step responses which can be defined as follow [20-22]:

$$Q = Q_o \sum_{i=1}^{4} (-1)^{n_i}\, u(t - a_i T) \qquad (2)$$

where $n_i = 0,\ 1,\ 2,\ 3;\ a_i = 0,\ 3,\ 5,\ 6.$

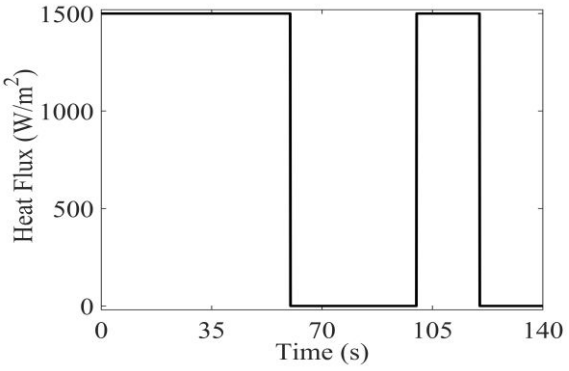

Fig.1 7-bit Barker coded thermal wave excitation used the numerical studies for defect detection in Ti-6Al-4V

Q -Thermal heat flux (W/m2); Q_o -Peak power of the heat flux (W/m^2); t -time (s); T- Total duration of the heat flux (s).

Boundary conditions at $x = L$ [23-27]:

$$Q(L,t) = -k\frac{\partial U(x,t)}{\partial x} = 0 \qquad (3)$$

Initial condition: *when*; $0 \le x \le L$; $t = 0$ [23-27]:

$$U(x,0) = U(x) = U_o = 293.15\ \text{K} \qquad (4)$$

The above Eq. (1) can be solved using Green's function approach for adiabatic boundary condition (presented by Eq. (2) and Eq. (3)) and constant initial condition (Eq. (4)). The overall obtained solutions can be written as [23-27]:

$$U(x,t) = U_o + \left(\frac{Q_o \alpha}{kL}\right)\sum_{i=1}^{4}\left[(-1)^{n_i}(t - a_i T)u(t - a_i T)\right] + \left(\frac{2Q_o}{kL}\right)\sum_{m=1}^{\infty}\left[\sum_{i=1}^{4}\left[\frac{(-1)^{n_i}}{\lambda_m^2}\cos(\lambda_m x)\left(1 - e^{-\alpha\lambda_m^2(t-a_i T)}\right)u(t - a_i T)\right]\right] \qquad (5)$$

where Eigenvalues - $\lambda_m = (m\pi/L)$; L- Specimen thickness; U_o -Initial temperature of the specimen

temporal thermal variation so depicted as a function of the hidden anomaly and the applied thermal excitation. The findings show that even with low peak power excitation sources, this thermographic technique with time-domain pulse compression approaches improves resolution compared to frequency domain approaches and results from high peak power, short duration pulsed excitation.

3 Pulse Compression Approaches for BCTWI Technique

By boosting the SNR of the response signals, time domain pulse compression of coded modulated signals via matched filtering, as employed in radar systems, improves the range resolution and sensitivity to offer improved subsurface fault identification even in randomly noisy situations. Depending on the temporal delay between the signals utilized, it focuses the energy that results from the application into a pseudo pulse whose peak concentrates at a delayed instant. As a result, new insight for coded modulation approaches was gained by probing via low peak powers and focusing energy in the main lobe similar to pulsed-based excitation schemes [28].

3.1 Frequency Domain Analysis

Fast Fourier Transform has been executed on the captured temporal thermal signature over the sample surface pixel by pixel for each pixel $g(x)$ in the field of view, as shown below [18, 19, 28].

$$Z(\omega) = \frac{1}{n}\sum_{i=0}^{n-1} g(x)\ e^{\left[\frac{-j2\pi\omega x}{n}\right]} = Re(\omega) + j\,Im(\omega) \qquad (6)$$

where, $R(\omega)$ is the real and $\mathrm{Im}(\omega)$ is imaginary parts of the Fast Fourier Transformed thermal data (ω); x represents the image sequence index.

Then, these obtained real and imaginary components of this FFT data of the captured thermal signature as shown in Eq. (6) can be utilized for the reconstruction of the phase images (Figure.2) as follow [19, 28]:

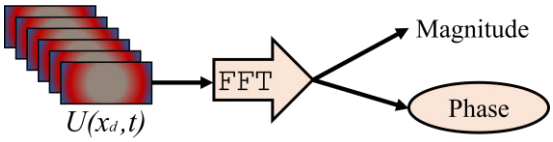

$U(x_d,t)$ - Thermal response at a given position
FFT - Fast Fourier Transform

Fig.2 The frequency domain processing approach flow chart adopted for construction of frequency domain phasegrams.

$$\varphi(\omega) = \mathrm{Tan}^{-1}\left(\frac{\mathrm{Im}(\omega)}{\mathrm{Re}(\omega)}\right) \tag{7}$$

3.2 Time Domain Analysis

The Hilbert transform (HT) analysis has been utilized to recover the time domain temporal temperature distribution's correlation coefficient and phase profiles [28-29]:

$$\mathrm{HT}(t) = \frac{1}{\pi}\int_{-\infty}^{\infty}\frac{U(x_r,\tau)}{t-\tau}d\tau \tag{8}$$

where, $U(x_r,\tau)$ is the selected reference thermal signal for the analysis. Then by utilizing the inverse fast Fourier transform (IFFT) properties, the cross-correlation coefficient (Figure.3) has been calculated as follows [29]:

Correlation coefficient

$$(CC) = \mathrm{IFFT}\left\{U(x_r,\omega)^* U(x_d,\omega)\right\} \tag{9}$$

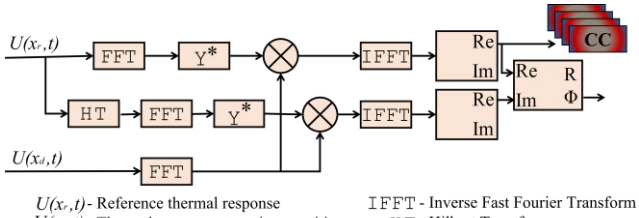

$U(x_r,t)$ - Reference thermal response
$U(x_d,t)$ - Thermal response at a given position
FFT - Fast Fourier Transform
IFFT - Inverse Fast Fourier Transform
HT - Hilbert Transform
Y^* - Complex Conjugate

Fig.3 Time domain processing approach flow chart adopted for construction of pulsed compressed correlation profiles and phasegrams

where $U(x_r,\omega)$ and $U(x_d,\omega)$ represent the Fourier transforms of the chosen reference thermal response and the temporal thermal response at a defect location, respectively. The time domain phase (Figure.3) has been reconstructed as follows by using the Fourier analysis [28, 29]:

$$\Phi = \mathrm{Tan}^{-1}\left(\frac{\mathrm{IFFT}\left\{\mathrm{HT}\,(\omega)^* U(x_d,\omega)\right\}}{\mathrm{IFFT}\left\{U(x_r,\omega)^* U(x_d,\omega)\right\}}\right) \tag{10}$$

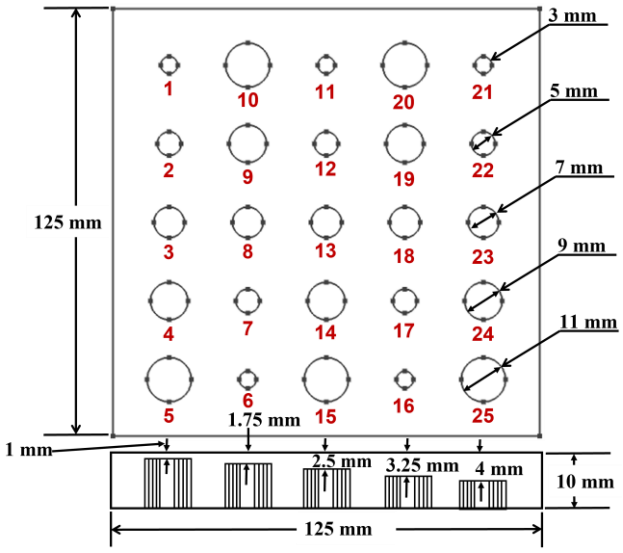

Fig.4 Schematic of modeled Titanium alloy Ti-6Al-4V with 25 flat bottom holes (FBH) used for defect detection analysis of BCTWI technique

Table.1 Thermal properties for Titanium alloy (Ti-6Al-4V) [1-6, 30]

Density (ρ) (kg/m^3)	**Specific heat capacity (C_p) (J/kg-K)**	**Thermal Conductivity (k) (W/m-K)**	**Thermal Diffusivity (α) (m^2/s)**
4512	570	7.3	$2.8384\ \ 0^{-6}$

4 Numerical Modeling and Simulation

A Titanium alloy (Ti-6Al-4V) specimen (Figure.4) with dimensions of 125×125×10 mm containing

twenty-five flat bottom hole defects was modeled and simulated for this investigation. The diameters of the modeled flat bottom holes are 3, 5, 7, 9, and 11 mm, respectively, which are at depths of 1, 1.75, 2.5, 3.25, and 4 mm for each diameter from the front surface of the test specimen (descripted in table.1). Figure.4 shows the schematic of this modeled test specimen with its specified dimensions. Table.1 summarizes the

Table.2 Description of flat bottom hole defects in modeled sample

Flat Bottom Hole (FBH) Diameters in millimetre	Flat Bottom Hole (FBH) Numbers as Mention in the figure.4				
	Defect depth (H) from specimen surface at: H1 = 1 mm	H2 = 1.75 mm	H3 = 2.5 mm	H4 = 3.25 mm	H1 = 4 mm
3 mm	1	6	11	16	21
5 mm	2	7	12	17	22
7 mm	3	8	13	18	23
9 mm	4	9	14	19	24
11 mm	5	10	15	20	25

thermophysical parameters of the investigated model. Then the numerical simulation studies had performed using finite element modeling and assessment software COMSOL Multiphysics with the heat transfer module in the solids. The modeled specimen consists of a finer mesh size with tetrahedral-shaped elements. The mesh comprises 96,775 domain elements, 16,918 boundary elements, and 1,679 edge elements.

Further, the specimen surface was exposed to Barker Coded thermal excitation (Figure.1) at 1500 W/m^2 for 140 seconds. Then the corresponding thermal signatures were recorded. These thermal data have been then processed with the time domain pulse compression-based data processing approaches to analyse the defect detection capability of the BCTWI technique in the Titanium alloy (Ti-6Al-4V).

5 Results and Discussions

A numerical simulation has been conducted to validate the defect detection capability of the purposed Barker-coded thermal wave imaging (BCTWI) modality in titanium-based alloys (Ti-6Al-4V). There are 25 flat bottom holes (FBH) modeled in the test specimen with different diameters at different depths, as shown in figure.4. Table 1 presents the thermophysical properties of the modeled titanium alloy specimen, Ti-6Al-4V. Subsequently, the Barker-coded excitation (Figure.1) was used to illuminate the sample's surface for 140 seconds.

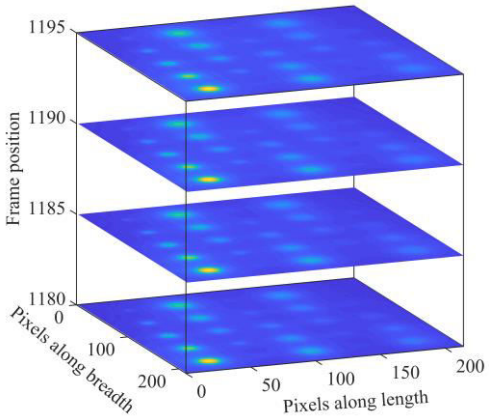

Fig.5 Raw temporal thermal profiles captured over the specimen surface

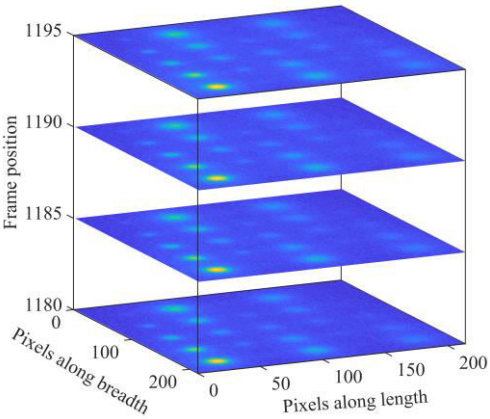

Fig.6 Raw temporal thermal profiles with added Additive White Gaussian Noise (AWGN) with an SNR of 20 dB

The resulting temporal thermal variation across the specimen surface was recorded at a frame rate of 20 Hz. These findings have presented in figure.5. The recorded raw thermal data was intentionally subjected to Additive White Gaussian Noise (AWGN) with an SNR of 20 dB to assess the suggested approach's detection potential under real-time conditions. The resulting noisy temporal thermal data (as shown in figure.6) is then processed using an appropriate polynomial fit of the first order to produce zero mean temporal thermal data. It is clear from the obtained fitted raw thermograms with added noise that the defects detectability at various depths of varying diameters is very difficult due to the insufficient thermal contrast provided over modeled specimen surface. Post-processing approaches such as frequency and time domain are employed to analyse this processed data.

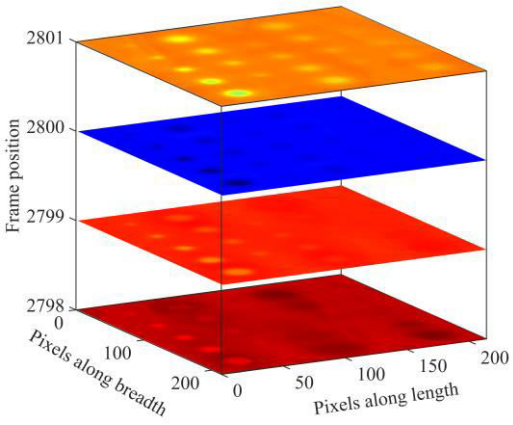

Fig.7 Schematic of phasegrams obtained using frequency domain analysis

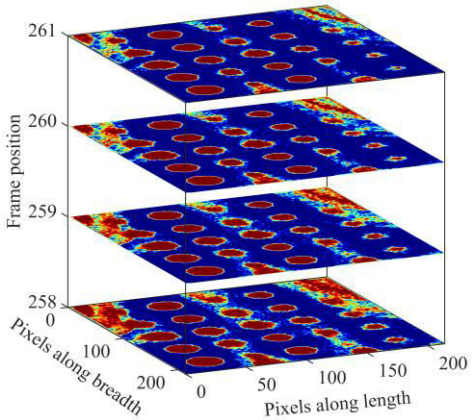

Fig.8 Schematic of phasegrams obtained using time domain analysis

Figure.7 shows the obtained frequency domain phase profiles constructed for different frames. The generated frequency domain phasegrams offer poor contrast over the test specimen surface and are not significant enough to reveal the defects at various depths with varying diameters.

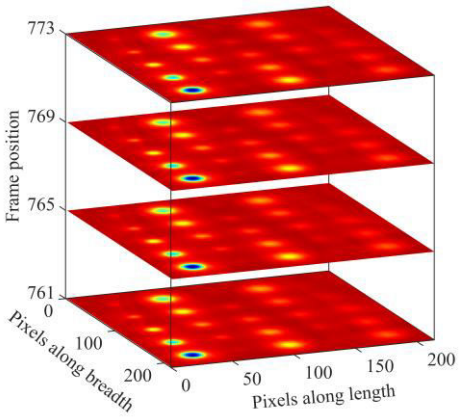

Fig.9 Schematic of correlation profiles obtained using matched filtered data processing approaches in time domain analysis

Further, figure.8 depicts the time-domain phasegrams obtained at different time steps using a cross-correlation-based post-processing approach. In contrast to this, figure.9 illustrates the constructed correlation coefficient profiles at different time instants from the matched filter-based data post-processing approach. The obtained time domain phase and correlation images show a noticeable contrast improvement in defect detection using the Barker-coded thermal wave imaging for the adopted time domain-based data processing methodologies.

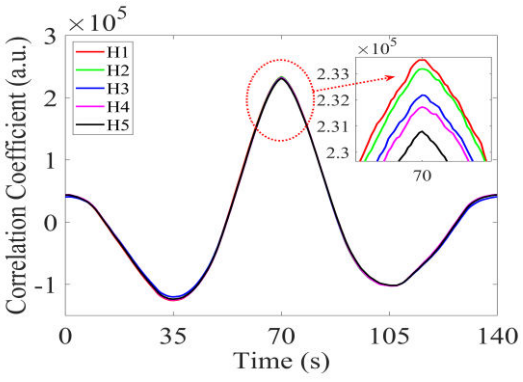

Fig.10a Single-pixel pulse compressed time domain correlation profiles for varying defects depths (H1, H2, H3, H4, and H5) as shown in Table.2 for 3 mm defect diameter

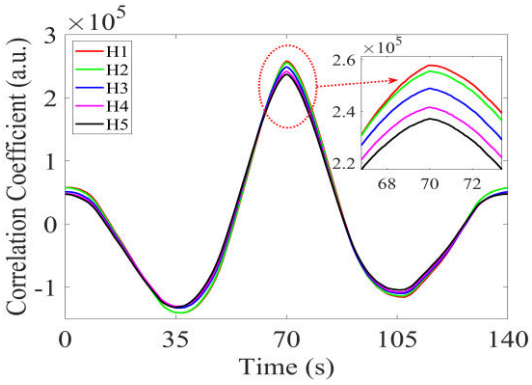

Fig.10b Single-pixel pulse compressed time domain correlation profiles for varying defects depths (H1, H2, H3, H4, and H5) as shown in Table.2 for 5 mm defect diameter

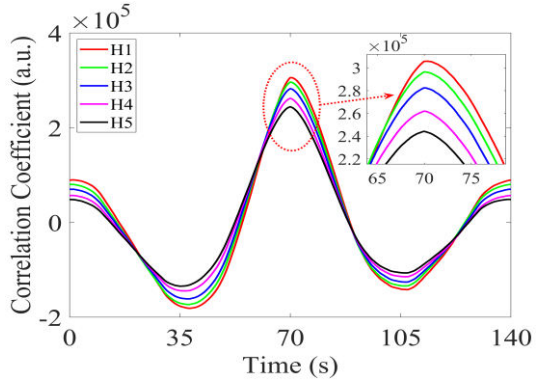

Fig.10c Single-pixel pulse compressed time domain correlation profiles for varying defects depths (H1, H2, H3, H4, and H5) as shown in Table.2 for 7 mm defect diameter

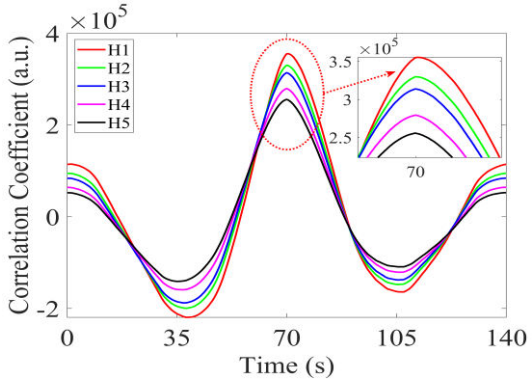

Fig.10d Single-pixel pulse compressed time domain correlation profiles for varying defects depths (H1, H2, H3, H4, and H5) as shown in Table.2 for 9 mm defect diameter

In addition, the single-pixel correlation coefficient profiles at the defect's centre shown in figure.10a, figure.10b, figure.10c, figure.10d, and figure.10e for the defect diameters 3 mm, 5 mm, 7 mm, 9 mm and 11 mm, respectively (pattern of the defects listed in

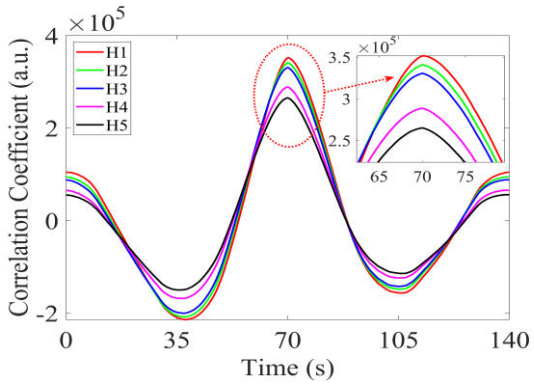

Fig.10e Single-pixel pulse compressed time domain correlation profiles for varying defects depths (H1, H2, H3, H4, and H5) as shown in Table.2 for 11 mm defect diameter

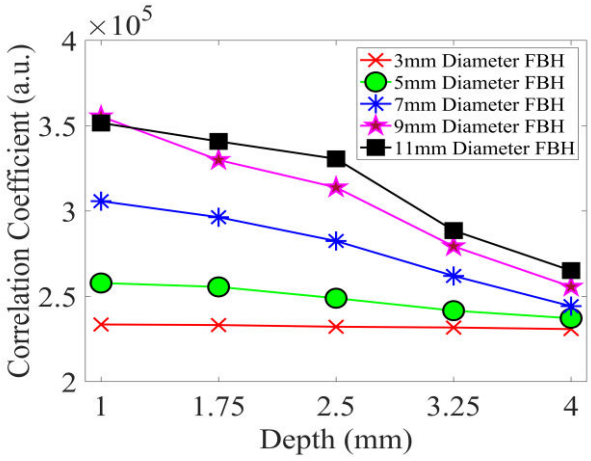

Fig.11 Schematic of time domain correlation coefficient versus defect depths in modeled Titanium alloy Ti-6Al-4V specimen for different defect diameters.

table.2). These computed single-pixel correlation profiles reveal that shallow depths have larger values than deeper depths. To examine the defect scanning capabilities of BCTWI modality employing matched filter-based data post-processing, the obtained single-pixel time-domain correlation coefficient values are plotted with regard to depths of defects of various sizes as shown in figure.11. The defects depth parameter presents over the x-axis, in contrast, the correlation coefficient standards over the y-axis as plotted in figureg.11. The correlation values show a monotonically declining trend as the depth of the defect from the sample surface increases for all faults with varied sizes. Hence, it can be concluded that the pulse compression-based time domain correlation approach is significant in the defect depth estimation in the Titanium alloy Ti-6Al-4V with the BCTWI technique.

6 Conclusions

Subsurface defect detection and estimation capability of the proposed Barker-coded thermal wave excitation has been presented for Titanium alloy Ti-6Al-4V. The results show that the suggested excitation approach with time domain correlation and phase-based data processing surpasses frequency domain-based phase analysis in terms of defect identification by producing the better thermal contrast in time domain. The results demonstrated that most of the energy focused in the main lobe creates a pseudo pulse through correlation, which improves defect detection in the correlation profiles. This approach also delivers improved defect depth resolution even with low peak power heat sources and a shorter code length. Furthermore, significant defects providing better thermal contrast, like phase contrast in time domain phase analysis, have also been observed.

7 References

[1] Dieter, G. E. (1986), "Mechanical Metallurgy", McGraw-Hill Book Company, New York, NY, USA

[2] Davis, J. R. (2003), "Handbook of Materials for Aerospace Engineering", Butterworth-Heinemann, Oxford, UK

[3] Gittos, M. F., & Smith, R. C. (1984), "Ultrasonic detection of defects in titanium alloys", Ultrasonics, 22(1), 11-19

[4] Evans, R. D., & Halbig, M. C. (1998), "Eddy current testing of titanium alloys", Materials Evaluation, 56(9), 1052-1056

[5] Bollinger, R. A., & McQuaid, R. A. (1983), "Magnetic particle inspection of titanium alloys", Materials Evaluation, 41(3), 342-345

[6] Lee, C. H., Lee, K., & Lee, S. H. (2018), "Nondestructive testing of titanium and titanium alloys", Metals, 8(7), 523

[7] Maldague, X. P. V. (2001), "Theory and practice of infrared technology for nondestructive testing", John Wiley & Sons

[8] Bahrami, M., & Bakhtiari-Nejad, F. (2013), "Applications of infrared thermography in nondestructive evaluation of materials: A review article", Journal of Nondestructive Evaluation, 32(2), 89-103

[9] Salazar, A., & Díaz, A. (2015), "Thermography as a non-destructive testing tool", Infrared Physics & Technology, 70, 28-47

[10] Fernández, F. F., López-Higuera, J. M., & Salgado, J. A. (2015), "Application of infrared thermography for defect detection in aerospace structures", Sensors, 15(9), 23549-23578

[11] Sakagami, T., and Kubo, S. (2002), "Applications of pulse heating thermography and lock-in thermography to quantitative non-destructive evaluations", Infrared Physics and Technology, vol. 43, no. 3-5, pp. 211-218

[12] Rosencwaig, A, (1982), "Thermal-wave imaging", Science, vol. 218, no. 4569, pp. 223-228

[13] Busse, G., and Eyerer, P. (1983), "Thermal wave remote and nondestructive inspection of polymers", Applied Physics Letters, vol. 43, no. 4, pp. 355-357, DOI: 10.1063/1.94335

[14] Dillenz, A., Zweschper, T., Riegert, G., and Busse, G. (2003), "Progress in phase angle thermography", Review of Scientific Instruments, vol. 74, no. 1 II, pp. 417-419

[15] Peng, D., and Jones, R. (2013), "Modelling of the lock-in thermography process through finite element method for estimating the rail squat defects", Engineering Failure Analysis, vol. 28, pp. 275-288

[16] Yang, R., and He, Y. (2016), "Optically and non-optically excited thermography for composites: A review", Infrared Physics & Technology, vol. 75, pp. 26-50

[17] Vavilov, V. P., and Marinetti, S.(1999), "Pulsed phase thermography and fourier-analysis thermal tomography", Russian Journal of Nondestructive Testing, vol. 35, no. 2, pp.134-145

[18] Maldague, X., and Marinetti, S. (1996), "Pulse phase infrared thermography", Journal of Applied Physics, 79 (5), pp. 2694- 2698

[19] Maldague, X., Galmiche, F., and Ziadi, A. (2002), "Advances in pulsed phase thermography", Infrared Physics and Technology, vol. 43, no. (3-5), pp. 175-181

[20] Mulaveesala, R., & Venkata Ghali, S. (2011), "Coded excitation for infrared non-destructive testing of carbon fiber reinforced plastics", Review of Scientific Instruments, 82(5), 054902

[21] Ghali, V.S., Panda, S.S.B., Mulaveesala, R. (2011), "Barker coded thermal wave imaging for defect detection in carbon fbre-reinforced plastics, Insight: Non-Destructive Testing & Condition Monitoring, vol. 53, No 11, pp. 621-624

[22] Dua, G., and Mulaveesala, R. (2013), "Applications of Barker coded infrared imaging method for characterisation of glass fibre reinforced plastic materials", Electronics Letters, 49 (17), pp. 1071-1073

[23] Carslaw, H. S., and Jaeger, J. C. (1959), "Conduction of Heat in Solids. Oxford Clarendon Press", London

[24] Özısık, M. N. (1993), "Heat conduction", John Wiley & Sons

[25] Sharma, A., Mulaveesala, R., Dua, G. and Kumar, N. (2020), "Linear frequency modulated thermal wave imaging for estimation of osteoporosis: An analytical approach", Electronics Letters, vol., 56, no. 19, pp. 1007-1010, doi: 10.1049/el.2020.0671

[26] Sharma, A., Mulaveesala, R., Dua, G., Arora, V. and Kumar, N. (2021), "Digitized Frequency Modulated Thermal Wave Imaging for Detection and Estimation of Osteoporosis", IEEE Sensors Journal, Article vol. 21, no. 13, pp. 14003-14010, Art. no. 9286563

[27] Sharma, A., Mulaveesala, R., and Arora, V. (2020), "Novel analytical approach for estimation of thermal diffusivity and effusivity for detection of osteoporosis", IEEE Sensors Journal, 20(11), pp. 6046-6054, doi:10.1109/JSEN.2020.2973233

[28] R Mulaveesala, J S Vaddi and P Singh (2008), "Pulse compression approach to infrared non-destructive characterisation", Review of Scientific Instruments, 79 (9), art no 094901

[29] N Tabatabaei, A Mandelis and B T Amaechi (2011), 'Thermophotonic radar imaging: an emissivity-normalised modality with advantages over phase lock-in thermography", Applied Physics Letters, 98 (16), art no 163706

[30] Sharma, A., Dua, G., Arora, V., Kumar, N., Mulaveesala, R. (2022), "A Novel Analytical Approach for Nondestructive Testing and Evaluation of Bone Implants Using Frequency Modulated Thermal Wave Imaging", Lecture Notes in Mechanical Engineering, pp. 273–285